Accepted Manuscript

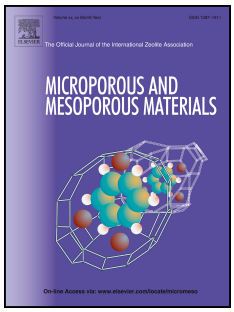

Methane hydrate formation in the confined nanospace of activated carbons in seawater environment

Carlos Cuadrado-Collados, François Fauth, Ión Such-Basañez, Manuel Martínez-Escandell, Joaquín Silvestre-Albero

PII: S1387-1811(17)30519-X

DOI: 10.1016/j.micromeso.2017.07.047

Reference: MICMAT 8476

To appear in: *Microporous and Mesoporous Materials*

Received Date: 8 June 2017

Revised Date: 19 July 2017

Accepted Date: 20 July 2017

Please cite this article as: C. Cuadrado-Collados, Franç. Fauth, Ió. Such-Basañez, M. Martínez-Escandell, Joaquí. Silvestre-Albero, Methane hydrate formation in the confined nanospace of activated carbons in seawater environment, *Microporous and Mesoporous Materials* (2017), doi: 10.1016/j.micromeso.2017.07.047.

TABLE OF CONTENTS IMAGE

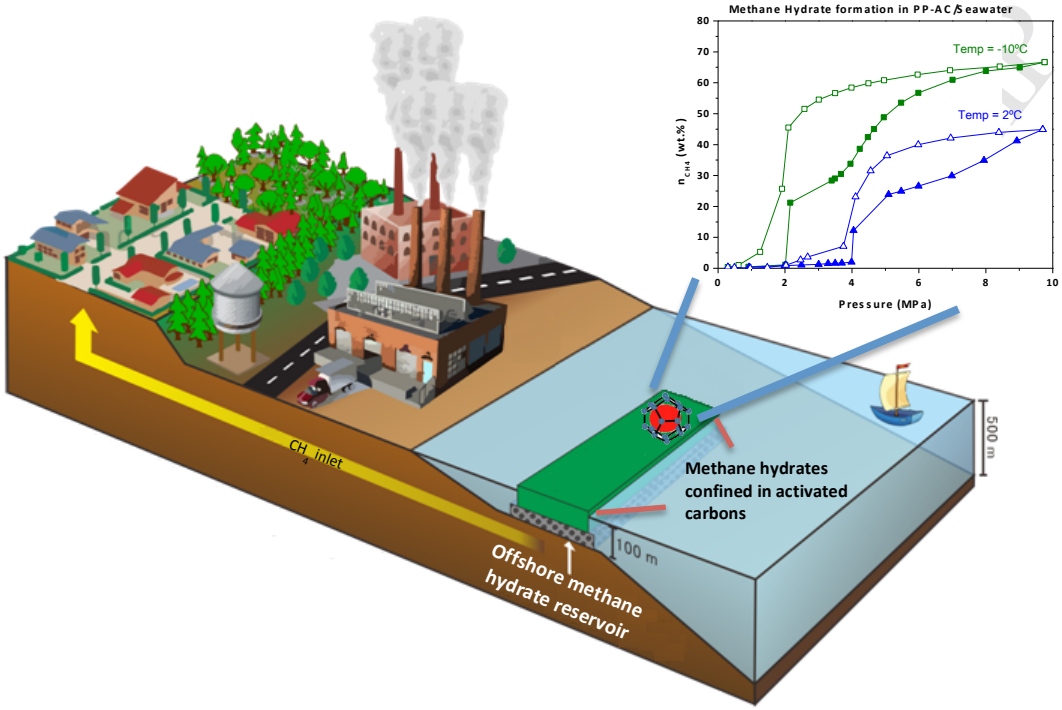

Methane hydrate formation in the confined nanospace of activated carbons in seawater environment

Carlos Cuadrado-Collados,[‡] *François Fauth,*[¥] *Ión Such-Basañez,*[§] *Manuel Martínez-Escandell,*[‡] *Joaquín Silvestre-Albero*[‡,*]

[‡] Laboratorio de Materiales Avanzados-Instituto Universitario de Materiales, Departamento de Química Inorgánica, Universidad de Alicante, Spain

[¥] CELLS-ALBA Synchrotron, E-08290 Cerdanyola del Vallés, Spain

[§] Servicios Técnicos de Investigación, Universidad de Alicante, Spain

Corresponding Author

*Email: joaquin.silvestre@ua.es

ORCID

Joaquín Silvestre-Albero: 0000-0002-0303-0817

ABSTRACT

Methane hydrate formation studies in saline environment show that activated carbons are excellent host structures able to promote the water-to-hydrate conversion. Under confinement conditions, methane hydrate formation takes place at mild temperatures (-10ºC), low pressures (< 6 MPa), with extremely fast kinetics (within minutes) and with a large adsorption capacity (up to 66 wt.% CH_4 for seawater, i.e. a 128% improvement compared to the dry carbon). Similar studies using ultrapure water give rise to a total methane adsorption capacity of 93 wt.%, i.e. entropic effects exerted by salt play a crucial role in the methane hydrate nucleation and growth. Synthesized methane hydrates exhibit a sI crystal structure and a stoichiometry that mimics natural hydrates. These findings open the gate towards the application of activated carbons with a highly developed nanoporous network as host structure for offshore methane storage in marine reservoirs.

KEYWORDS: Gas hydrates, methane storage, nanoconfinement, activated carbon, saline environment.

1. INTRODUCTION

Strong economic growth and expanding population in non-OECD nations is expected to increase energy demand more than 71% from 2012 to 2040, and around 18% in mature energy-consuming and slower-growing OECD economies [1]. Taking into account actual oil depletion and the intermittent regime of renewable sources, there is an urgent need to

find alternative energy sources able to fulfill these stringent requirements for the next decades. Methane, the main component of natural gas, is regarded as a prospective alternative to petroleum because of its higher specific combustion enthalpy and the lower emission of carbon dioxide upon combustion relative to petroleum [2]. Actual prospections have estimated vast deposits of methane in the form of gas hydrates at the permafrost in the Artic regions (*ca.* 8%) and in deep marine water environments (*ca.* 92%), the amount of methane stored estimated by the DOE (US Department of Energy) being around $3x10^{15}$ cubic meters or ≅1800 Gt of carbon. For instance, countries like Japan (M21 research consortium) successfully extracted methane as a fuel through thermal stimulation of natural gas hydrates in 2012.

This nature-inspired approach has been recently proposed as an excellent alternative to store large amounts of methane for mobile and stationary applications, provided that artificial gas hydrates can be prepared under mild pressure and temperature conditions and with reasonable kinetics (short charging time) [3]. Considering that 1 cm^3 of gas hydrate is able to store 164 cm^3 of methane, artificial methane hydrates can be applied in cylindrical vessels to store methane in small-scale devices (e.g., transportation) or for long-term methane storage in off-shore artificial marine platforms, as a safe supply for highly demanding nations. Although bulk nucleation of gas hydrates is a kinetically-limited process that hinders their commercial exploitation, a number of studies described in the literature have anticipated that the nucleation induction period can be drastically decreased from weeks down to minutes upon incorporation of a solid surface, for instance activated carbons, silicas or metal-organic frameworks (MOFs) [4-12]. The presence of proper

liquid-framework interactions and a large specific interphase area between the gas and water on the solid surface promotes the nucleation and growth of artificial gas hydrates at milder conditions (2ºC and 2-4 MPa) than nature, and with faster kinetics than bulk and natural hydrates [4,5]. Despite the importance of this technological approach for future storage devices, all studies described in the literature have concentrated in ideal conditions using ultrapure water as liquid media. However, the scenario changes drastically in the case of using the hydrate technology to design future long-term storage reservoirs under artificial marine platforms located at the coastline (around 100 m depth). To tackle this complex idea it is necessary to get new knowledge into the methane hydrate formation process in saline environments. Although there are already several studies in the literature dealing with the effect of salinity in bulk hydrate formation [13,14], to our knowledge there are no studies dealing with their growth in saline environments under confinement conditions, i.e. nucleation in the confined space of nanoporous solids.

With this in mind, the aim of the present study is to evaluate the methane hydrate nucleation and dissociation process in the confined nanospace of a high-surface area activated carbons using seawater from the Pacific Ocean. Nucleation kinetics, pressure threshold, stability and stoichiometry of the hydrate will be evaluated at different temperature and pressure conditions. The selection of Pacific Seawater (Fiji Island) is based on the potential interest of the surrounding countries (mainly China and Japan) to exploit this hydrate technology in their coasts.

2. EXPERIMENTAL

The activated carbon PP-AC was prepared using a mesophase pitch (VR-vacuum residue) as a carbon precursor. The synthesis process involves a pyrolysis step at 460ºC under 1 MPa of N_2 for 1.5h. The resulting pitch has a mesophase content around 93%. After the pyrolysis, the pitch was grounded in a ball mill to obtain a particle size below 500 μm. The powder was activated with KOH as a chemical agent in a 6:1 ratio (wt.%/wt.%) at 800ºC for 2h under a nitrogen flow of 100 ml/min (heating rate 5ºC/min). The obtained activated carbon was washed first with a HCl solution (10 wt.%) and finally with distilled water. The final sample, labeled PP-AC, was dried overnight at 100ºC.

The morphology of the synthesized activated carbon has been evaluated using field emission scanning electron microscopy (FESEM model ZEISS Merlin VP Compact). Temperature-programmed decomposition analysis (TPD) was performed in a U-shape flow-reactor (He flow 50 ml/min) connected on-line to a mass spectrometer (MS). The amount of oxygen surface groups evolved as CO and CO_2 has been quantified after appropriate calibration of the MS using calcium oxalate. DSC measurements were performed in a DSC Q100 apparatus (TA Instruments) using hermetically sealed aluminum pans. A typical experiment consists of a cool-heat cycle under 50 ml/min N_2. The sample is first cooled from 20ºC to -80ºC at a heating rate of 1ºC/min, then the temperature is hold isothermal for 5 minutes and finally a heating rate of 1ºC/min is used to heat the sample back to 20ºC.

Textural properties of the synthesized samples were evaluated by gas physisorption of nitrogen at -196 ºC. Gas adsorption measurements were performed in a homemade fully automated manometric equipment designed and constructed by the Advanced Materials

Group (LMA), now commercialized as N2GSorb-6 (Gas to Materials Technologies; www.g2mtech.com). The sample was previously degassed for 4 h at 250 ºC under vacuum (10^{-3} Pa). Nitrogen adsorption data were used to determine the following: (i) the total pore volume (Vt) at a relative pressure of 0.95, (ii) the BET-specific surface area (S_{BET}) and (iii) the micropore volume (V_{N2}) by application of Dubinin–Radushkevich equation. The difference between V_t and V_{N2} is considered to be the mesopores volume (V_{meso}).

To make the hydrate structures, the nanoporous carbon sample was pre-humidified under water-supplying conditions denoted by Rw (Rw, which represents the mass of water to dry carbon). The Rw value selected is 4.1, that corresponds to the oversaturated sample (saturation capacity measured using water adsorption at 25ºC is 1.8 g/g). CH_4 adsorption/desorption capacity was measured at 2ºC and -10ºC and up to 10 MPa. Pre-humidified samples were frozen at -20 ºC before the outgassing treatment to avoid water loss.

Synchrotron X-ray powder diffraction (SXRPD) experiments were collected at the high-pressure/microdiffraction end station of the MSPD beamline at synchrotron ALBA in Spain. Data were collected at 0.4243Å wavelength using a Rayonix SX165CCD 2D detector. The experiments were performed on an ad hoc capillary reaction cell (fused silica capillary, inner diameter 0.7 mm, outer diameter 0.85 mm). Before the experiment, the H_2O pre-impregnated (4.1 g_{H2O}/g_{AC}) carbon (either pure water or seawater) was placed inside of the capillary connected to the methane gas cylinder (purity 3.5) via a pressure regulator. An Oxford Cryostream 700 was used to control the temperature of the sample. In situ XRPD measurements were performed at 0 and 5 MPa of methane and different temperatures, from -10ºC up to 2ºC.

3. RESULTS AND DISCUSSION

3.1. Sample Characterization

Table S1 reports the composition of the seawater and the conductivity. The salinity of the Fiji seawater is between 38.6 and 39.3, as deduced from the compositional analysis and the conductivity, respectively. A high-surface area activated carbon (AC) derived from petroleum pitch (PP) after activation with KOH was used as a host structure. PP-AC was prepared using the recipe described by Casco et al., the resulting sample combining a large apparent BET surface area (above 3400 m^2/g) and a highly developed microporous (V_0 = 1.00 cm^3/g) and mesoporous (V_{meso} = 1.42 cm^3/g) structure (Figure S1) [4]. In addition, Hg porosimetry shows a wide macropore size distribution, ranging from 0.1-100 μm, coming from the removal of the activating agent [4]. The morphology of the synthesized activated carbon has been evaluated using FESEM. As it can be observed in Figure S2, activated carbon grains have a dense packed structure with clearly visible μm size cavities or holes due to the removal of KOH after the activation treatment. These large cavities constitute the pathways to reach the inner micropores in the activated carbon.

The amount and type of oxygen surface groups have been evaluated by temperature-programmed decomposition (TPD) experiments (Figure S3). TPD profile shows a small evolution of acidic groups, evolved as CO_2 ([CO_2] = 0.235 mmol/g), in the temperature range 400-800 K (mainly attributed to carboxylic and lactone surface groups), and the subsequent evolution of the less acidic groups evolved as CO at higher temperatures (mainly attributed to phenol, carbonyl and quinone groups) [CO] = 0.807 mmol/g. The amount of groups evolved as CO is larger than those evolved as CO_2, as corresponds to

activated carbon materials, although the total amount released is not large, i.e. the synthesized petroleum-pitch derived activated carbon (PP-AC) has a poor surface chemistry.

3.2. Differential Scanning Calorimetry

The understanding of any crystallization phenomena upon a thermal stimuli in a confined environment, for instance in the cavities of a nanoporous solid, is a complex process that deserves special attention before evaluating the hydrate formation process. Thermodynamically, any fluid in a confined pore width (H) experiences a modification in the chemical potential that shifts the freezing temperature respect to the bulk (ΔT_f), the direction of the shift (positive or negative) depending on the wall-solid (γ_{ws}), the latent heat of melting in the bulk (λ_{fb}), and the wall-fluid (γ_{wl}) surface tensions, for a given molar volume of the liquid (ν) (Gibbs-Thomson (GT) equation (1)).

$$\frac{\Delta T_f}{T_{fb}} = -2\frac{(\gamma_{ws} - \gamma_{wl})\nu}{H\lambda_{fb}} \qquad (1)$$

According to the literature, for repulsive or weakly attractive potentials, the shift in the freezing temperature ΔT_f must be negative while for strongly attracting walls an increase must be observed [15-17]. Furthermore, the shift is predicted to be larger for slit versus cylindrical pores [18]. These studies confirmed the success of the Gibbs-Thomson equation down to about 8 nm pores, the linear behavior between ΔT_f and 1/H breaking down for smaller pores. This observation was attributed to the presence of a contact surface layer

within the pore with different dynamic and structural properties compared to the pore-interior, so that this contact layer become relevant for narrow pores [15]. Figure 1 shows the differential scanning calorimetry (DSC) profiles for the melting of bulk water (ultrapure and seawater) and the PP-AC confined water (4.1 g_{H2O}/g_{AC}). DSC scans for the freezing step are shown in the Supporting information (Figure S4).

DSC profiles for the freezing and melting of bulk H_2O differs significantly due to the presence of kinetic restrictions during the freezing step. In the freezing process (Figure S4) there is a clear shift to lower temperatures for seawater, both in the bulk and the confined phase, compared to pure water systems due to entropic effects of salt in the disorder (liquid) to order (solid) transition. In any case, the presence of the activated carbon promotes the nucleation of ice crystals at higher temperatures compared to the bulk, the degree of sub-cooling required being smaller. As described above, the freezing process in the DSC is kinetically controlled by the nucleation and crystal growth of ice, thus yielding a metastable super-cooled fluid below its freezing temperature, while the melting process is under thermodynamical control and no metastable phases are observed. A closer look to the melting scans in Figure 1 show important differences between bulk pure and seawater. Pure water exhibits a single perfectly symmetric endothermic peak with an onset temperature of 0.08ºC and associated with a latent heat of fusion of 330 J/g (see Table S2), in perfect agreement with the theoretical value for pure water.

Concerning the seawater, DSC curves exhibit three endothermic contributions at -36.9ºC, -23.9ºC and -5.0ºC and associated with a total enthalpy value of 270 J/g. These observations show that entropy has two effects, a decrease in the melting temperature and a decrease in the enthalpy, i.e. less energy is required to melt ice in seawater. The peaks at low

temperatures in seawater could be attributed to the melting of the outermost water layers due to the weakening of the hydrogen-bonded structure in the presence of salt (the transition from cubic to hexagonal ice can be ruled out since it must take place at temperatures below the range evaluated, ca. -80ºC to -50ºC) [19,20].

Concerning the confined phase, pure water exhibits a single peak at -0.1ºC, with a small shoulder at lower temperatures. Compared to the bulk, confined water exhibits a decrease in the melting temperature, in close agreement with the Gibbs-Thomson equation for weakly interacting systems. The asymmetry at lower temperatures denotes the presence of a second contribution attributed to the melting of H_2O in pores of different size [20,21]. The presence of two peaks associated with the melting of H_2O in different pores can also be appreciated for the confined seawater. However, compared to the bulk seawater, the confined peaks are shifted to higher temperatures. Taking into account that pore size (H) is common in Figure 1, the positive shift in the confined seawater clearly denotes a difference in the surface tensions (slightly attracting interactions) in the presence of salt.

Last but not least it is important to highlight that the enthalpies of melting, normalized per gram of H_2O (see Table S2), are much lower for the confined system compared to the bulk, in close agreement with previous studies by Kaneko et al. [15,22]. Apparently, the enthalpy change in the transition from the crystal phase to the orientationally ordered confined liquid is considerably reduced in the confined environment.

3.3. High-Pressure Methane Isotherms

Upon understanding the confinement effects in the freezing/melting process, the oversaturated PP-AC samples (4.1 g_{H2O}/g_{AC}; pure and seawater) have been evaluated in the

methane hydrate formation. Figure 2 shows the methane adsorption/desorption isotherms at 2ºC and -10ºC and up to 10 MPa.

As it can be observed, at 2ºC and below 3 MPa, the amount of methane adsorbed is almost zero due to the pore blocking by pre-adsorbed water. In the specific case of pure water, the methane adsorption capacity at 2ºC exhibits a drastic jump at 3.2 MPa that continues up to 6 MPa. Above this threshold pressure there is a second jump in the methane adsorption capacity up to 10 MPa and associated with a large hysteresis loop. The final adsorption capacity for methane at 10 MPa is as high as 76 wt.%, large above the adsorption capacity for the dry sample (26 wt.%) [4]. As reported elsewhere, these two steps in the methane adsorption/desorption isotherm reflect the methane hydrate formation process in large cavities or in the external surface area (first step) and in the inner porosity (second step) [4]. Interestingly, the scenario changes drastically in the case of confined seawater. Below 4 MPa neither methane adsorption nor methane hydrate formation takes place. Above this pressure, two steps can be appreciated, a first one between 4 and 6 MPa, and the second one from 6 to 10 MPa. These results clearly anticipate a few findings, i) the presence of salty water shifts the methane hydrate formation to higher pressures, ii) the water-to-hydrate yield decreases in the presence of seawater (amount adsorbed at 10 MPa is 45 wt.%, still quite above the dry sample), iii) the lower yield is mainly due to the limited hydrate formation in the second step (41% decrease in the methane adsorption capacity), i.e. the inhibition effect of seawater is larger in the inner cavities or small pores of the activated carbon, and iv) the presence of salt also alters the dissociation of the methane hydrate, taking place at higher pressures (≅ 3.8 MPa). The larger stability of pure methane hydrate

versus seawater hydrate in confined nanospace is in close agreement with previous studies in bulk phase [13]. Tishchenko et al. predicted a relationship between the increase in the methane dissociation pressure in the bulk and the seawater salinity [14]. The inhibition of the hydrate formation process in the inner pores of the carbon material when using seawater can either be due to the blocking effect exerted by salt in these cavities or to thermodynamic concerns, i.e. entropic effects in the presence of salt as deduced before with DSC. To answer the first question, the textural properties of sample PP-AC have been evaluated after the hydrate formation process using N_2 adsorption at cryogenic temperatures. N_2 adsorption isotherm after the methane hydrate formation using pure water (Figure S1) is perfectly coincident with that of the original PP-AC, with a S_{BET} above 3400 m^2/g. In the case of seawater, the N_2 adsorption isotherm exhibits a certain blocking effect due to the salt, preferentially in the large micropores and small mesopores region, the S_{BET} decreasing down to 2850 m^2/g. However, the blocking of the porosity (16% decrease in total pore volume) is not enough to explain the large inhibition in the hydrate formation process at pressures above 6 MPa. To answer the second question, the methane adsorption/desorption isotherms have been evaluated quite below the melting temperature, i.e. at -10ºC. As it can be observed in Figure 2 (bottom), both pure and seawater pre-impregnated PP-AC exhibit a similar behaviour. At -10ºC, 2 MPa is the threshold pressure for both systems with a sudden jump in the amount adsorbed up to a similar value (ca. 22-25 wt.%), i.e. entropic effects are minimized at low temperatures. Afterwards, both samples exhibit a second step attributed to hydrate formation in smaller cavities up to a final amount adsorbed as high as 93 wt.%, for pure water, and 66 wt.%, for seawater. Compared to the adsorption capacity of the dry carbon at -10ºC (29 wt.%), the incorporation of water gives

rise to a 220% (pure water) and 128% (seawater) improvement in the methane adsorption capacity per mass of dry carbon. Apparently, temperatures below the melting point i) promote the methane hydrate formation at lower pressures for both steps, ii) minimize the entropic effects exerted by seawater both for the hydrate formation and dissociation, and iii) give rise to an improved water-to-hydrate yield, preferentially in the confined seawater [23]. At this point it is important to highlight that seawater could never reach the adsorption capacity of pure water because the more water is converted to hydrate, the more the concentration of salt solution becomes, with the associated larger inhibition due to the lower solubility of methane in saline water.

In summary, these results suggest that high-surface area activated carbons are promising candidates to promote methane hydrate formation under mild conditions (low pressures and moderate temperatures) either with pure water or seawater. Although, confined seawater exhibits a certain inhibition, these thermodynamic effects can be largely minimized at temperatures slightly below the melting point.

Stoichiometry of the methane hydrate has been estimated from the amount of methane adsorbed up to 10 MPa and the total amount of water pre-impregnated. As it can be appreciated in Table S3, pure water gives rise to an excess of methane both at 2ºC and -10ºC compared to the theoretical stoichiometry for natural hydrates (1 $CH_4 \cdot 5.75\ H_2O$) [3]. However, a careful evaluation of the two steps in the isotherm (Table S3) suggests that the first step, attributed to methane hydrate formation in large cavities, is indeed in perfect agreement with the theoretical value, while the hydrates formed in the second step are the ones being non-stoichiometric. These results can be explained either due to the non-stoichiometry of the hydrates in narrow pores due to steric restrictions or most probably to

the presence of physisorbed methane non participating in the hydrate process. Physisorbed CH_4 at -10ºC has been estimated to be around 29.3 wt.%. Under seawater environment the scenario is quite different. While at -10ºC there is a perfectly stoichiometric hydrate formation (preferentially in the first step), all calculations performed at 2ºC clearly anticipate an excess of water compared to methane, i.e. the water-to-hydrate yield must be quite low under these circumstances, in close agreement with the results in Figure 2 at 2ºC.

3.4. Methane Adsorption kinetics

Despite the total adsorption capacity, another important parameter in the hydrate formation process is the nucleation and growth kinetics. Figure S5 shows the variation in the sample cell pressure versus time for specific points at the methane adsorption isotherms described in Figure 2, i.e. (a) right after the first step and (b) in the inflexion point of the second step, for the pure water and seawater confined samples. Kinetic measurements described in Figure S5a show that the first step, corresponding to methane hydrate formation in large cavities or external surface area, exhibit a certain induction period (ca. 1-6 h) before the nucleation step starts for measurements at 2ºC. Interestingly, the induction period is much shorter in saline environments probably due to salt acting as the nucleation sites. Importantly, a decrease in the adsorption temperature below the melting point minimizes the differences between pure and seawater and reduces the induction period ca. 20 min. After the induction period, nucleation starts with more than 80% equilibrium reached after 5h for both pure and seawater. Concerning the second step in the isotherm at aprox. 5-6 MPa (at 2ºC) and 3-4 MPa (at -10ºC), kinetic measurements clearly anticipate the absence of any induction period. Methane hydrate nucleation and growth takes place right after the

expansion of the gas manifold with equilibrium times of a few hours (between 5-20h) depending on the adsorption temperature. In other words, methane hydrate nucleation in the inner cavities of the activated carbon, although it is a slow process, does not require an induction period. This observation must be due to the over-pressure required, compared to hydrates in the external surface or large cavities, and the associated larger amount of methane dissolved. At this point it is important to emphasize that similar experiments in the absence of activated carbon do not provide any adsorption at all even after 1-2 weeks, thus confirming the promoting role of the confined nanospace.

3.5. Synchrotron X-Ray Powder Diffraction (SXRPD)

Last but not least, the nature of the methane hydrate has been evaluated using in-situ synchrotron X-ray powder diffraction at the MSPD end-station of the ALBA synchrotron (Spain). SXRPD patterns have been measured before and after methane pressurization up to 5 MPa for PP-AC confined pure and seawater. As it can be observed in Figure 3, upon a cooling step at -10ºC both pure water and seawater give rise to the characteristic peaks of the hexagonal structure of ice. The subsequent pressurization with methane up to 5 MPa gives rise to the development of new peaks associated to the sI methane hydrate, together with ice. The co-existence of both phases must be associated with the low equilibrium time allowed during consecutive SXRPD measurements. However, a slight increase in the capillary temperature to 2ºC speeds up the methane hydrate formation process with a pure sI structure for both pure and seawater. These results clearly confirm that the crystal structure of the methane hydrate is independent of the environment, saline or not, the sI structure being the most stable structure, with complete absence of unreacted ice. The

crystal size estimated from the SXRPD measurements is rather similar for methane hydrate coming from pure and seawater, the average crystal size being around 100 nm, i.e. using synchrotron XRD only large crystals, those in large pores or cavities, can be identified. The crystallite size of the hydrate was calculated based on Scherrer equation and using LaB_6 NIST 660b as a standard for instrumental peak broadening determination

4. CONCLUSIONS

High-pressure (up to 10 MPa) methane hydrate adsorption/desorption experiments clearly show that high-surface area activated carbon materials are excellent host structures to promote the methane hydrate nucleation and growth. These crystalline structures exhibit a sI structure and are successfully synthesized under mild pressure and temperature conditions either in pure water or seawater. The effect of a saline environment depends on the nucleation temperature. Whereas at temperatures above the melting point salt shifts the nucleation process to higher pressures and promotes the dissociation at higher pressures, at temperatures below the melting point these two processes are rather similar to pure water, i.e. the inhibition effect by salt can be minimized. Interestingly, seawater-based hydrate synthesized at -10ºC exhibits extremely fast kinetics (only a few minutes) and a stoichiometry that mimic nature. In any case, the total methane adsorption capacity in a saline environment, although very large (up to 66 wt.%), cannot reach the one of pure water (93 wt.%) due to entropic and blocking effects associated with the presence of salt.

ASSOCIATED CONTENT

Supporting Information. Characterization of the PP-AC sample, characterization of seawater and adsorption kinetics.

ACKNOWLEDGMENT

Authors acknowledge financial support from MINECO: Projects MAT2016-80285-P and CONCERT Project-NASEMS (PCIN-2013-057), and Generalitat Valenciana (PROMETEOII /2014/004). J.S.A. also acknowledge the Spanish synchrotron ALBA for beam time availability (Project 2016021724).

REFERENCES

[1] DOE/EIA-0484. International Energy Outlook 2016, pp. 1-84.

[2] K. Vasanth Kumar, K. Preuss, M.M. Titirici, F. Rodríguez-Reinoso, Chem. Rev. 117 (2017) 1796-1825.

[3] E.D. Sloan, C.A. Kohn, Clathrate Hydrates of Natural Gases, 3rd Ed., CRC Press, 2007.

[4] M.E. Casco, J. Silvestre-Albero, A.J. Ramirez-Cuesta, F. Rey, J.L. Jordá, A. Bansode, A. Urakawa, I. Peral, M. Martinez-Escandell, K. Kaneko, F. Rodríguez-Reinoso, Nature Commun. 6 (2015) 6432.

[5] M.E. Casco, J.L. Jordá, F. Rey, F. Fauth, M. Martinez-Escandell, F. Rodríguez-Reinoso, E.V. Ramos-Fernandez, J. Silvestre-Albero, Chem. Eur. J. 22 (2016) 10028 - 10035.

[6] M.E. Casco, F. Rey, J.L. Jordá, S. Rudic, F. Fauth, M. Martinez-Escandell, F. Rodríguez-Reinoso, E.V. Ramos-Fernández, J. Silvestre-Albero, Chemical Science 7 (2016) 3658-3666.

[7] A. Celzard, J.F. Marêché, Fuel 85 (2006) 957-966.

[8] A. Perrin, A. Celzard, J.F. Marêché, G. Furdin, Energy Fuels 17 (2003) 1283-1291.

[9] W. Wang, C.L. Bray, D.J. Adams, A.I. Cooper, J. Am. Chem. Soc. 130 (2008) 11608-11609.

[10] L. Yan, G. Chen, W. Pang, J. Liu, J. Phys. Chem. B 109 (2005) 6025-6030.

[11] V. Govindaraj, D. Mech, G. Pandey, R. Nagarajan, J.S. Sangwai, J. Natural Gas Sci. & Tech. 26 (2015) 810-818.

[12] A. Siangsai, P. Rangsunvigit, B. Kitiyanan, S. Kulprathipanja, P. Linga, Chem. Eng. J. 126 (2015) 383-389.

[13] V. Kumar Saw, I. Ahmad, A. Mandal, G. Udawabhnu, S. Laik, J. Natural Gas Chem. 21 (2012) 625-632.

[14] P. Tishchenko, C. Hensen, K. Wallmann, C. Shing Wong, Chem. Geol. 219 (2005) 37-52.

[15] R. Radhakrishnan, K.E. Gubbins, A. Watanabe, K. Kaneko, J. Chem. Phys. 111 (1999) 9058.

[16] K. Overloop, L. Van Gerven, J. Magn. Reson., Ser. A 101 (1993) 179.

[17] K. Morishige, K. Kawano, J. Chem. Phys. 110 (1999) 4867-4872.

[18] M. Maddox, K.E. Gubbins, J. Chem. Phys. 107 (1997) 9659-9667.

[19] M.A. Sanchez, T. Kling, T. Ishiyama, M.-J. van Zadel, P.J. Bisson, M. Mezger, M.N. Jochum, J.D. Cyran, W.J. Smith, H.J. Bakker, M.J. Shultz, A. Morita, D. Donadio, Y. Nagata, M. Bonn, E.H.G. Backus, PNAS 114 (2017) 227-232.

[20] M. Sliwinska-Bartkowiack, M. Jazdzewska, L.L. Huang, K.E. Gubbins, Phys. Chem. Chem. Phys. 10 **(**2008) 4909-4919.

[21] M.R. Landry, Thermochimica Acta 433 **(**2005) 27-50.

[22] K. Kaneko, A. Watanabe, T. Iiyama, R. Radhakrishnan, K.E. Gubbins, J. Phys. Chem. 103 (1999) 7061-7064.

[23] L. Borchardt, W. Nickel, M.E. Casco, I. Senkovska, V. Bon, D. Wallacher, N. Grimm, S. Krause, J. Silvestre-Albero, Phys. Chem. Chem. Phys. 18 (2016) 20607-20614.

FIGURE CAPTION

Figure 1. DSC scans for melting of H_2O (ultrapure and seawater) in the bulk (bottom) and confined (4.1 g_{H2O}/g_{AC}) in the PP-AC sample (upper).

Figure 2. CH_4 adsorption/desorption isotherms at 2ºC (upper) and -10ºC (bottom) for ultrapure and seawater pre-impregnated PP-AC (4.1 g_{H2O}/g_{AC}). The total adsorption capacity at 10 MPa for the dry carbon at both temperatures is also included.

Figure 3. Synchrotron X-ray powder diffraction patterns for pure and seawater confined in PP-AC; (a) H_2O at 2ºC, (b) H_2O at -10ºC, (c) H_2O at -10ºC and 5 MPa CH_4 and (d) same conditions of (c) at 2ºC.

FIGURES

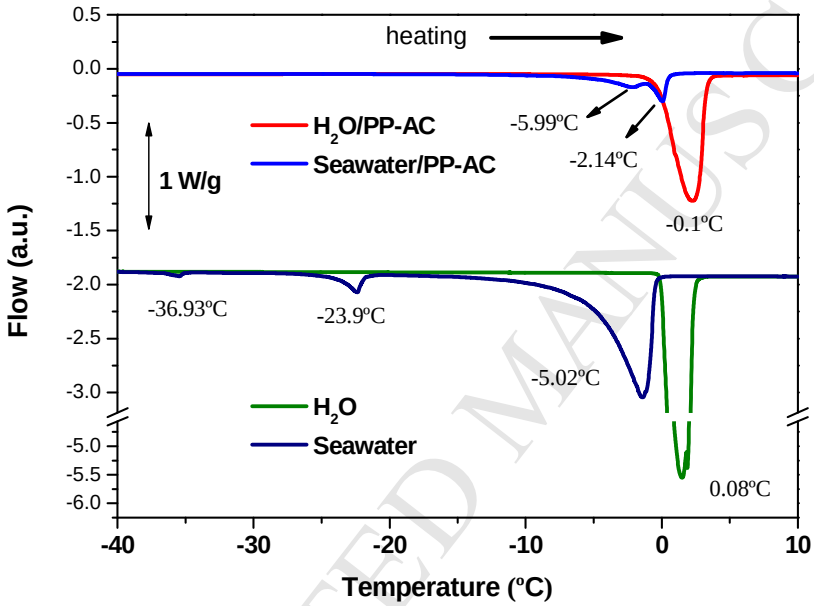

FIGURE 1

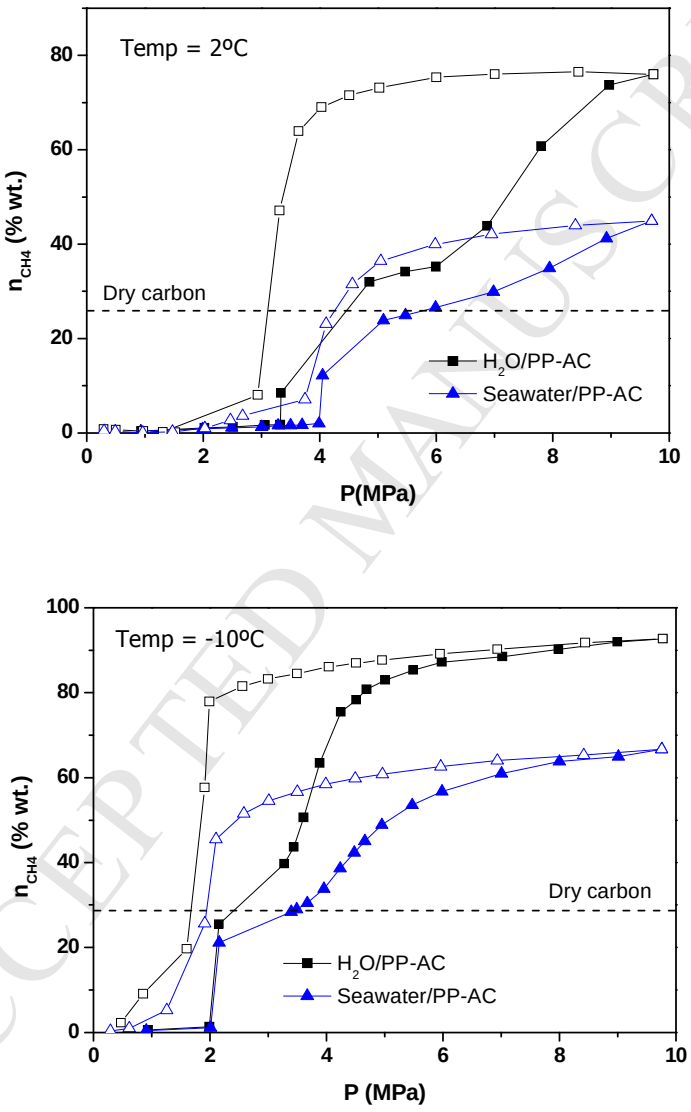

FIGURE 2

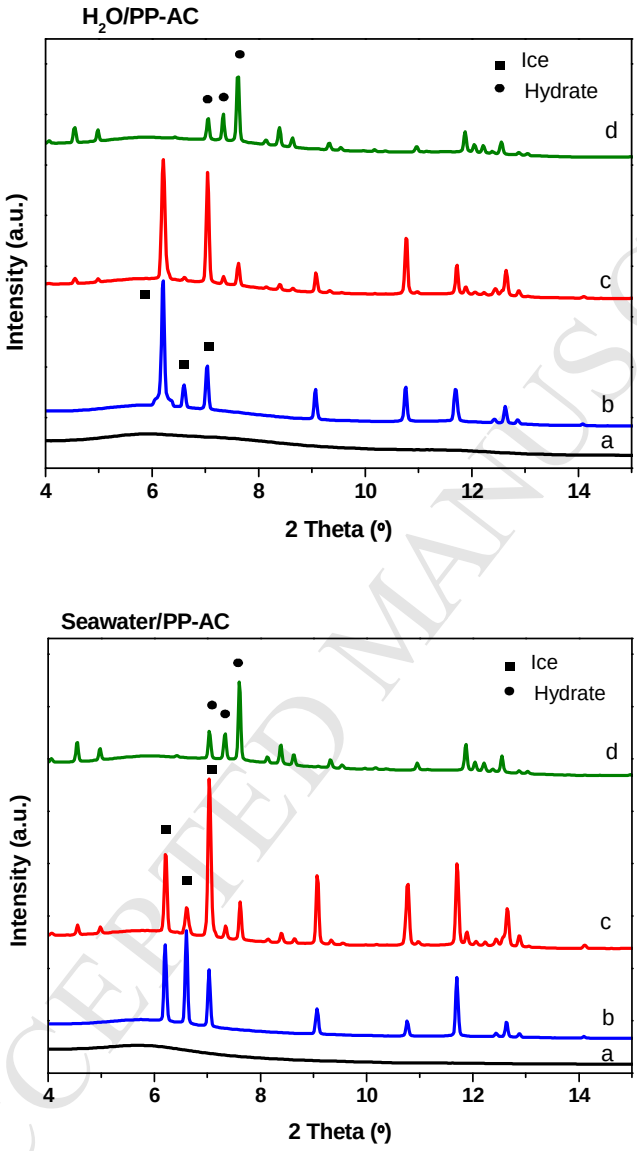

FIGURE 3

Highlights

- Nanoconfinement effects promote methane hydrate formation in seawater environment
- Methane adsorption capacity in seawater is improved more than 128%
- Presence of salt limits the water-to-hydrate yield above the melting temperature
- Confined seawater-based gas hydrates have similar stoichiometry to natural hydrates